

1 **Highlights**

- 2 1. Global extinction strain rate (a_g) decreases with increase in porous burner
3 diameter (D).
- 4 2. Plug flow condition is valid for oxidizer inlet distance > 2 times the largest
5 porous burner diameter.
- 6 3. CO/H₂ mixtures diluted with N₂ yield 1.6–2.25 times higher a_g in com-
7 parison to CO/H₂ mixtures diluted with CO₂.
- 8 4. Overall reaction rate (ω_o) is used to explain variation in a_g values with
9 compositions.

10 Effect of burner diameter and diluents on the extinction
11 strain rate of syngas-air non-premixed Tsuji-type flames

12 S M Ali^{a,*}, S Varunkumar^b

13 ^a*Department of Aerospace Engineering, Indian Institute of Technology Madras, Chennai -*
14 *600 036*

15 ^b*Department of Mechanical Engineering, Indian Institute of Technology Madras, Chennai -*
16 *600 036*

17 **Abstract**

18 The present study focuses on the experimental determination of the global ex-
19 tinction strain rate (a_g) for different syngas-air combinations using the Tsuji
20 type configuration. To study the effect of porous burner diameter (D), a_g values
21 were obtained for four values of D at atmospheric pressure. The experimentally
22 obtained a_g for a given fuel-oxidizer combination decreases with an increase in
23 burner diameter (D). This trend is consistent with the limited data available
24 in the literature for hydrocarbon fuels. Other geometric and flow-field effects
25 namely, (1) plug flow, (2) flow-field blocking by the burner, and (3) heat loss
26 by the flame to sidewalls that can affect a_g were also experimentally quantified.
27 The results from this study show that the plug flow boundary condition is al-
28 ways satisfied for oxidizer inlet distance > 2 times the largest porous burner
29 diameter. Burner diameter less than $1/4$ times side wall length (as is the case
30 for all burners used in this study) does not significantly modify the flow. Hence,
31 these two flow-field modifications do not affect a_g . However, heat loss from the
32 flame to the ambient through the side walls can cause a 4-9 % decrease in a_g .
33 Experiments showed that, CO/H₂ mixtures diluted with N₂ yield 1.6–2.25 times
34 higher a_g in comparison to CO/H₂ mixtures diluted with CO₂. Increasing H₂
35 from 1 to 5 % leads to 2.5–3.8 times increase in a_g , compared to 5 to 10 %
36 increase in H₂ which leads to only 1.3–1.7 times increase in a_g for 70 % of N₂
37 (v/v) in fuel mixture. Global extinction strain rate (a_g) increases by 1.5–2.4
38 times with 10 % increase in CO for fuel mixtures consisting of H₂ (1 and 5

*Corresponding author
Preprint submitted to International Journal of Hydrogen Energy
Email address: smughees.ali@gmail.com (S M Ali)

39 % by v/v), CO₂ (50, 60 and 70 % by v/v) and N₂ (50, 60, 70 and 80 % by
40 v/v). The change in overall reactivity (ω_o) due to different diluents is used to
41 quantitatively explain the variation of a_g for different fuel compositions. These
42 effects are also qualitatively explained using OH radical concentration change
43 with H₂ % in the fuel mixtures.

44 *Keywords:* Tsuji-type configuration; syngas-air non-premixed flames; global
45 extinction strain rate (a_g); burner geometry effect; diluents effect

46 1. Introduction

47 Gasification, a widely used thermo-chemical route for conversion of biomass
48 and coal yields fuel gases rich in carbon monoxide and hydrogen (called syngas
49 or producer gas). The composition of the syngas produced from gasification is
50 highly variable. It strongly depends on the oxidizer composition used for gasifi-
51 cation, which is generally a mixture of O₂/N₂/CO₂/steam; fuel composition also
52 affects the syngas composition, though not as strongly as oxidizer composition.
53 ([1–3]).

54 Syngas utilization devices vary a lot in terms of applications. For instance,
55 gas-turbines used in IGCC ([4, 5]), reciprocating engines used for decentralized
56 power generation ([6–8]), gasifier based improved biomass stoves ([9, 10]) etc.
57 Therefore, extensive data on the behavior of premixed and non-premixed syngas
58 flames, covering a range of CO/H₂ ratios and different inert species are essential
59 for the development of syngas based combustion devices. For the determination
60 of syngas premixed flame characteristics, a significant number of computational
61 and experimental studies were performed in the past ([11–21]). Yepes and Amell
62 [22], Bouvet et al. [23] and Varghese et al. [18] have experimentally obtained
63 laminar flame speed for wide range of syngas compositions using Bunsen burner
64 configuration and heated divergent channel method respectively. The 1D nu-
65 merical computations performed by Yepes and Amell [22] and Varghese et al.
66 [18] using the available kinetic mechanisms showed reasonably accurate pre-
67 dictions for laminar flame speeds. Unlike the case for non-premixed flames,

68 these studies predict premixed flame characteristics are under reasonable accu-
69 racy. For instance, Bilger [24] has calculated global kinetic parameters using
70 Tsuji [25] data for methane-air non-premixed flames. He has concluded that
71 the conditions for the non-premixed flames are different from those in plug flow
72 and well-stirred reactor, and therefore, rate parameters calculated from these
73 reactors should not be used for non-premixed flames. Results from CFD sim-
74 ulations of the Sandia-ETH Zurich turbulent syngas jet diffusion flames ([26])
75 using eight kinetic mechanisms (three simplified and five detailed) reported by
76 Marzouk and Huckaby [27] show that, none of the mechanism is capable of
77 predicting the temperature and species concentration profiles accurately. So,
78 for accurately predicting the temperature and species concentration profiles in
79 syngas non-premixed flames, the syngas kinetic mechanism must be optimized
80 using non-premixed syngas flame data. Extinction strain rate (a) is used to
81 characterize non-premixed flames. The focus of the current work is to charac-
82 terize syngas non-premixed flames for various fuel-oxidizer compositions using
83 the extinction strain rate (a).

84 Extinction strain rate (a) is defined as the component of the velocity gradient
85 normal to the flame surface at extinction. Similar to laminar flame speed (S_L)
86 for the premixed flames, extinction strain rate (a) is an important characteristic
87 of non-premixed flames. Two types of measurements are commonly used to
88 characterize flame extinction, (1) the local extinction strain rate (a_l), and (2)
89 the global extinction strain rate (a_g). The local extinction strain rate (a_l) is
90 defined as the maximum velocity gradient normal to the flame surface just
91 upstream of the thermal layer on the oxidizer side ([28]). The global extinction
92 strain rate (a_g) is defined as the strain rate on the oxidizer side close to the
93 stagnation plane, assuming self-similarity and zero radial gradients of all scalar
94 variables along the axis of symmetry ([29]).

95 To experimentally obtain the a_g and a_l , two counterflow configurations
96 namely, (1) opposed jet flow and (2) Tsuji-type are commonly used. Based
97 on nozzle geometry, the opposed jet counterflow configuration can be further
98 divided into straight and contour nozzle type configurations. The other con-

99 figuration used to obtain a_g and a_l is the Tsuji type burner, in which flame
 100 extinction is achieved near the stagnation point of oxidizer flow past a porous
 101 cylinder issuing fuel (see Fig. 1).

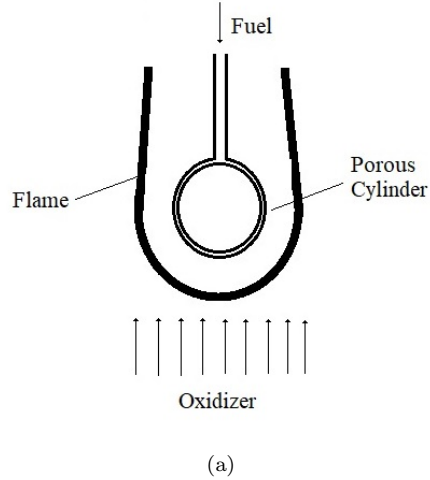


Figure 1: Schematic of Tsuji-type configuration

102 This counterflow configuration is known as the Tsuji type burner as it was
 103 extensively used by Tsuji and co-workers to perform flame extinction experi-
 104 ments on gaseous fuels starting from 1960 till 1985 (see refs. [25, 30, 31]). For
 105 this configuration, global extinction strain rate (a_g) is given by Eqn. 1.

$$a_g = \frac{4u_{ox}}{D} \quad (1)$$

106 where, u_{ox} is the free stream oxidizer velocity at extinction and D is the diameter
 107 of the porous burner issuing fuel. The following assumptions are used in deriving
 108 Eqn. 1 - (1) potential flow, (2) change in the location of the stagnation plane due
 109 to blowing at extinction is minimal, (3) flow field modification at the oxidizer
 110 side of stagnation plane due to flame is neglected, and (4) flame surface is close
 111 to stagnation plane ([31]). In both configurations, flame extinction is achieved
 112 by increasing the total mass flow rate. The location of the flame is determined
 113 by the stoichiometry and jet momentum ratio in the axial direction.

114 In the past decade, a significant number of computational and a few exper-
115 imental studies are performed for syngas non-premixed flames in opposed jet
116 configurations. The focus of these studies are primarily in three different areas
117 namely, (1) determination of NO_x emission characteristics ([32–38]), (2) effect
118 of diluent like CO_2 , H_2O and N_2 on flame structure ([39–42]) and (3) deter-
119 mination of extinction strain rate (a) for wide range of syngas compositions
120 ([33, 43–46]).

121 Park and co-workers ([39, 40, 42]) have computationally studied the effect of
122 radiation, preferential diffusion and reactivity of diluent on non-premixed flame
123 structure for different syngas compositions. For the cases without and with
124 radiation, Park et al. [39] have found a difference of more than 100 K in flame
125 temperatures at low strain rate ($\leq 10 \text{ s}^{-1}$). However, this difference reduces
126 to less than 30 K at high strain rate value ($\geq 100 \text{ s}^{-1}$). In 1D computations,
127 Park et al. [40] have modified the diffusivity of H_2 to be equal to the diffusivity
128 of N_2 and studied its effect on flame temperature and overall reactivity. As
129 N_2 is less diffusive in comparison to H_2 , they have termed it as suppression
130 of H_2 diffusivity. Their study on the effect of H_2 diffusivity on syngas non-
131 premixed flame structure showed that, suppression of H_2 diffusivity should not
132 only be considered as the physical change ([40]). The higher diffusivity of H_2
133 also kinetically modifies the syngas non-premixed flame structure. Park et al.
134 [42] have shown that, CO_2 cannot be considered as completely inert and CO_2
135 mole fraction is reduced by reverse CO hydroxyl path oxidation ($\text{CO}_2 + \text{H} \leftrightarrow$
136 $\text{CO} + \text{OH}$). Fu et al. [47] have studied the effect of preferential diffusion and
137 flame stretch on the structure of premixed Bunsen syngas flames. They have
138 found out that, for high H_2 % in fuel the flame structure is affected by flame
139 curvature and preferential diffusion.

140 Hsin and co-workers have computationally studied the effect of composi-
141 tion, pressure and dilution on the structure of syngas non-premixed flames
142 ([41, 43, 45]). Shih and Hsu [41] have shown, among the four effects of dilu-
143 ent (inert, diffusion, chemical and radiation), the inert effect is dominant in
144 reducing flame temperature. Flame temperature decreases with an increase in

145 volumetric diluent percentage and as expected based on the specific heat val-
146 ues, the maximum decrease in a_g was observed for CO₂, followed by H₂O and
147 N₂. Shih and Hsu [43] results show that, at low strain rate ($\leq 10 \text{ s}^{-1}$), H₂
148 is consumed before CO but the flame cannot be distinguished as two separate
149 flames. Shih et al. [45] have also found out for very low strain rate (1 s^{-1}),
150 only 0.002 % of H₂ is required for stable CO/H₂ flame. This study also shows
151 that flame cannot exist for an equimolar mixture of CO/H₂ for O₂ less than
152 4.7 % by volume in oxidizer stream at any strain rate value. Their observation
153 of reduction in flame temperature by radiation at low strain rate is consistent
154 with that of Yang and Shih [37]. Also, their observation about the chemical and
155 inert effect of diluent is found to be consistent with Park et al. [42] and Sahu
156 and Ravikrishna [33]. Important to note that, all these studies conducted by
157 Park's ([39, 40, 42]) and Shin's ([41, 43, 45]) group on the effect of diluents on
158 syngas non-premixed flames are for low to moderate global strain rate 10–100
159 s^{-1} . In these studies, the effect of diluents on extinction was not investigated.

160 Sahu and Ravikrishna [48] have performed extinction strain rate study for
161 both premixed and non-premixed syngas flames using contour nozzle type op-
162 posed jet configuration. They have shown that, global extinction strain rate
163 (a_g) decreases with an increase in nozzles separation distance (L), while the
164 local extinction strain rate (a_l) does not significantly vary with L . Hence, Sahu
165 and Ravikrishna [48] have used a_l for comparison of experiments with 1D com-
166 putations. Prediction of a_g from 1D computations assumes plug flow boundary
167 condition, i.e., zero velocity gradient (du/dx) in the axial direction at fuel and
168 oxidizer nozzles exit. However, Kee et al. [49] have concluded that, plug flow
169 assumption is not always valid and for predicting flame extinction accurately,
170 realistic boundary conditions are to be employed. The experimental data of
171 Sahu and Ravikrishna [48] shows a significant value for du/dx (15–40 % of a_l)
172 at the fuel and oxidizer nozzles exit.

173 In Table 1, relevant results from earlier studies on opposed jet non-premixed
174 syngas flames along with the available geometric parameters are compiled. For
175 non-premixed syngas flames, data show that, out of five, three kinetic mech-

176 anisms namely, Li et al. [50], GRI Mech 3.0 ([51]) and Frassoldati et al. [20]
177 can predict local extinction strain rate (a_l) for low H_2/CO ratio, but all these
178 kinetic models fail to predict a_l for high H_2/CO ratio. The maximum difference
179 in a_l values from experiments and 1D computations is found to as high as 25
180 % ([48]). Study performed by Som et al. [38] using three kinetics mechanisms
181 (GRI Mech 3.0, Davis et al. [52] and Mueller et al. [53]) for non-premixed and
182 partially premixed flames has shown that the kinetic model proposed by Davis
183 et al. [52] to be most accurate. For premixed flames Sahu and Ravikrishna [48]
184 have shown that, kinetic models of Davis et al. [52] and Frassoldati et al. [20]
185 predicts a_l under 10 % accuracy for all H_2/CO composition used. The data show
186 that the predicted a_l values for the premixed syngas flames are more accurate
187 in comparison to non-premixed syngas flames. As most of these kinetic mecha-
188 nisms are optimized using the premixed flame characteristics, it is possible that
189 these kinetic mechanisms predict a_l values more accurately for premixed flame
190 in comparison to non-premixed flames. Bilger [24] has developed the global
191 kinetic mechanism for CH_4 oxidation by analyzing the methane non-premixed
192 data obtained using the Tsuji configuration. He has found out a significant
193 difference in the kinetic parameters calculated using non-premixed Tsuji config-
194 uration from that of the well-stirred (Dryer and Glassman [54]) and plug flow
195 reactor (Williams et al. [55]). Bilger [24] has concluded that the conditions for
196 a non-premixed flames are different from those in plug flow and well-stirred re-
197 actor and therefore, rate parameters calculated from these reactors should not
198 be used for non-premixed flames.

Table 1: Summary of the a_g and a_l for the two opposed jet configurations. Error value is estimated by symbol size if in case not provided. Extinction strain rate values in italics with “*” represents a_l , BCs:- Boundary conditions, var:- Variable

Fuel (% by volume)	Configuration $L(\text{mm})/D(\text{mm})$ Contour Nozzle	Experiments a_g or a_l (s^{-1})	1D computation a_g or a_l (s^{-1}) BCs (Potential)
Sahu and Ravikrishna [48]			
35CO/05H ₂ /02CH ₄ /58N ₂	17/30	1230±25	-
	17/30	<i>619*±25</i>	<i>500*,520*,608*,539*,681*</i>
32CO/08H ₂ /02CH ₄ /58N ₂	7/30	2497±210	-
	7.5/30	2158±308	-
	8/30	2141±325	-
	12/30	1928±277	-
	-/-	<i>826*±33</i>	<i>687*,683*,794*,779*,911*</i>
29CO/11H ₂ /02CH ₄ /58N ₂	-/-	<i>966*±38</i>	<i>966*,922*,1024*,1068*,1168*</i>
26CO/14H ₂ /02CH ₄ /58N ₂	10.5/30	2411±39	-
26CO/14H ₂ /02CH ₄ /58N ₂	-/-	<i>1149*±45</i>	<i>1235*,1201*,1284*,1357*,1460*</i>
23CO/17H ₂ /02CH ₄ /58N ₂	-/-	<i>1773*±70</i>	<i>1543*,1542*,1602*,1657*,1758*</i>
20CO/20H ₂ /02CH ₄ /58N ₂	-/-	<i>2300*±90</i>	<i>1842*,1944*,1954*,1964*,2091*</i>
Wang et al. [46]			
	Straight nozzle	Uniform	2D Computations
Syn1-60N2	10.2/10.2	820±136	<i>643,661*</i>
Syn1-65N2	10.2/10.2	647±70	<i>408,413*</i>
Syn1-70N2	10.2/10.2	461±86	<i>214,221*</i>
		Parabolic	
Syn1-50N2	10.2/11.2	860±63	<i>777,735*</i>
Syn1-55N2	10.2/11.2	645±45	<i>537,581*</i>
Syn1-60N2	10.2/11.2	460±50	<i>322,382*</i>
Syn1-65N2	10.2/11.2	311±50	<i>158,224*</i>
Syn1-70N2	10.2/11.2	179±41	<i>95,109*</i>
Syn2-60N2	10.2/11.2	856±66	<i>752,736*</i>
Syn2-65N2	10.2/11.2	625±50	<i>398,481*</i>
Syn2-70N2	10.2/11.2	365±45	<i>180,235*</i>
Syn2-75N2	10.2/11.2	200±54	<i>80,89*</i>

199 The two possible reasons for the difference in a_l values between experimental
200 and 1D computations are uncertainties in determination/optimization of trans-
201 port properties and kinetic parameters. Sahu and Ravikrishna [48] have stated
202 that, “differences of 15 % and higher are observed in predictions of extinction
203 strain rates by the various mechanisms despite the use of similar transport li-

204 braries.” From this, Sahu and Ravikrishna [33] has concluded that improvement
205 in both kinetic parameter and transport properties are required for better pre-
206 diction of extinction of non-premixed flames.

207 Wang et al. [46] have obtained global extinction strain rate (a_g) experimen-
208 tally and compared them with 2D axisymmetric computations for syngas non-
209 premixed opposed jet flames. They have used two different types of boundary
210 conditions (parabolic and uniform) to obtain a_g and compared them with 2D
211 computations. Using 2D axisymmetric computations, they have shown that, the
212 difference in assumed and actual axial centerline velocity increases with an in-
213 crease in global strain rate for parabolic inflow velocity. However, for uniform
214 inflow axial velocity, a constant difference of about 16 % between assumed and
215 actual centerline axial velocity is observed for three global strain rate values.
216 The computational data of Wang et al. [46] shows a constant difference of about
217 16 % between assumed and actual centerline axial velocity which is due to en-
218 forcement of ideal uniform axial velocity profile at a distance of 5.1 mm from
219 the nozzle exit. Wang et al. [46] have concluded that, “it is very doubtful that
220 the matrix is capable of producing such a uniform flow profile in the actual
221 experiments, particularly for elevated flow conditions.” Hence, for accurately
222 predicting a_g , idealized velocity profiles (parabolic or uniform) at the nozzles
223 exit can not be used. The analysis of Wang et al. [46] data from Table 1 shows
224 that, indeed 2D axisymmetric computations are able to predict the trends, but
225 under-predict a_g values for all the fuel-air compositions used. The maximum
226 difference in a_g values from experiment and 2D computation is found out to be
227 as high as 60 %.

228 The other simplified geometry used to study non-premixed flames is Tsuji-
229 type configuration. This configuration has an advantage over opposed-jet coun-
230 terflow configuration in terms of flow field modification by the flame near the
231 oxidizer inlet. In Tsuji-type configuration, if the oxidizer boundary is placed
232 sufficiently far from the burner, it will not interact with flame. One of the
233 objectives of the current work is to determine this minimum distance between
234 the oxidizer boundary and the porous cylinder burner. Tsuji and co-workers

235 ([25, 30, 31]) have obtained a_g values experimentally for CH_4 and C_3H_8 , but to
236 the best of our knowledge, we have not come across any study on determination
237 of a_g for different CO/H_2 compositions.

238 In the current study, a_g values are experimentally obtained using Tsuji type
239 configuration for a range of syngas compositions with N_2 and CO_2 as diluents.
240 The composition range covered in this study is - CO from 10 to 49 % (v/v), H_2
241 from 1 to 10 % (v/v), N_2 dilution of 20 to 50 % (v/v) and CO_2 dilution of 30-50
242 % (v/v). The choice of the composition range investigated here is based on
243 the following considerations- (1) very high to low CO/H_2 ratios (49–1) diluted
244 with CO_2 and N_2 , (2) syngas compositions obtained using $\text{O}_2/\text{N}_2/\text{CO}_2/\text{steam}$
245 as oxidizer for biomass gasification ([1, 2, 9, 10, 56]) (3) few compositions were
246 chosen from the study of Wang et al. [46] to compare the a_g values obtained
247 from Tsuji burner with opposed jet configuration.

248 **2. Experimental Methodology**

249 A schematic of the counterflow Tsuji type burner setup used in the current
250 work is shown in Fig. 2. The burner is designed according to the dimensions
251 proposed by Tsuji and Yamaoka [30]; an additional flow-straightener is used
252 just after the convergent nozzle for ensuring uniform laminar flow. The details
253 of the design are explained below.

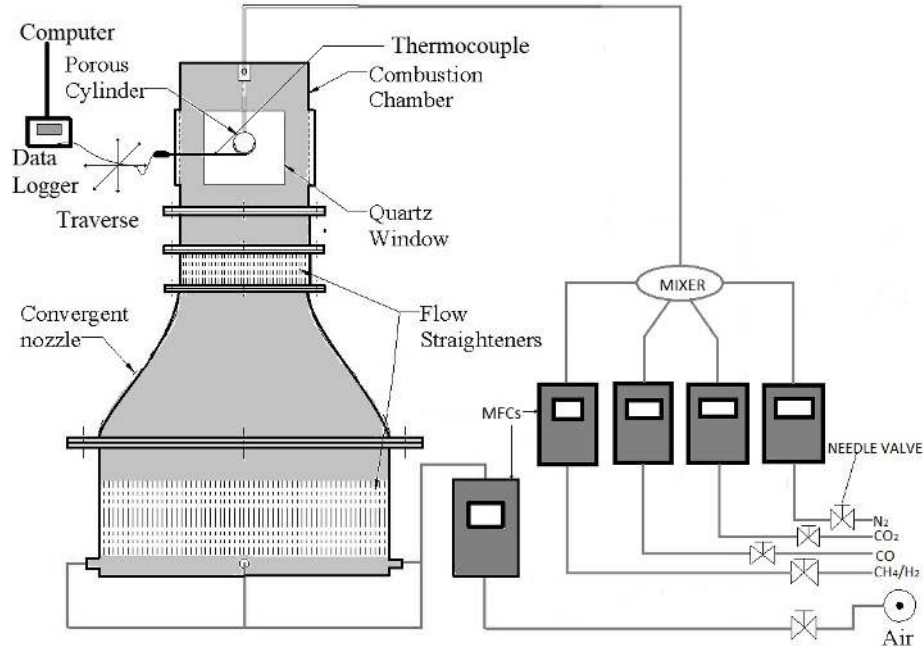


Figure 2: Schematic of the experimental setup

254 The counterflow setup consists of five parts, namely, the combustion cham-
 255 ber, porous cylinder, flow straighteners, convergent nozzle and the settling cham-
 256 ber. The combustion chamber (12 cm × 25 cm × 3 cm) ($l \times h \times w$) was fixed
 257 with quartz windows (10 cm × 10 cm) along its length for flame visualization.
 258 The sides of the combustion chamber consist of two slots (10 cm × 2.5 cm) which
 259 were generally closed but can be open when required. The porous cylinder was
 260 fixed inside the combustion chamber with a holding mechanism such that the
 261 distance of the porous cylinder burner from the bottom of the combustion cham-
 262 ber can be varied. Fuel was discharged only from the porous area of the burner
 263 that is $\pi/3$ degrees on either side of the stagnation point. The sidewall openings
 264 in the combustion chamber were covered with a wire mesh and the porous cylin-
 265 der burner was kept at a distance of 12 cm from the bottom of the combustion
 266 chamber (oxidizer inlet) unless otherwise mentioned. Four porous cylinders of
 267 length 3 cm and diameters 10.6 mm, 15.6 mm, 22.8 mm and 30.8 mm were used

268 for the experiments. The bottom section of the combustion chamber is attached
269 to a straight rectangular duct of 5 cm height. This duct is further attached to
270 flow straighteners of 5 cm height. These flow straighteners consist of a bundle
271 of metal tubes of diameter 0.25 mm and length 5 cm which maintain a laminar
272 flow at the duct exit. The lower section of these flow straighteners was attached
273 to a convergent rectangular nozzle connected to the settling chamber (25 cm ×
274 25 cm × 25 cm). The settling chamber was also fixed with flow straighteners to
275 reduce local turbulence and maintain uniform laminar flow at the nozzle entry.

276 For metering and controlling the fuel and air supply, mass flow controllers
277 with an accuracy of 1 % of the full-scale reading was used. Fuel gases were
278 supplied from pressurized gas cylinders fixed with a two-stage pressure regulator.
279 An upstream pressure of 5 bar was maintained just before gas filters. Gas filters
280 of 5 μm mesh size were fixed upstream of the MFCs to remove any particulate
281 impurity coming from the pressurized fuel gas cylinders. Carbon monoxide,
282 hydrogen, carbon dioxide, nitrogen with 99.9 % and methane with 99.5 % purity
283 levels were mixed in different proportions and used as fuel. Experiments were
284 conducted with methane (pure and diluted with N_2) and syngas (with different
285 CO/H_2 ratios) diluted with N_2 and CO_2 . The fuel compositions used in this
286 study are listed in Table 2.

Table 2: Nomenclature for CH₄/N₂ and CO/H₂/N₂/CO₂ blends used as fuel. *All % are in volumetric basis

Nomenclature	CH ₄ (%)*	CO (%)	H ₂ (%)	CO ₂ (%)	N ₂ (%)
CH ₄	100	0	0	0	0
CH ₄ -30N ₂	70	0	0	0	30
CH ₄ -50N ₂	50	0	0	0	50
CH ₄ -70N ₂	30	0	0	0	70
Syn1-55N ₂	0	22.5	11.25	11.25	55
Syn1-65N ₂	0	17.5	8.75	8.75	65
Syn2-60N ₂	0	15	15	10	60
Syn2-70N ₂	0	11.25	11.25	7.5	70
Syn-5H ₂ 80N ₂	0	15	5	0	80
Syn-10H ₂ 80N ₂	0	10	10	0	80
Syn-1H ₂ 70N ₂	0	29	1	0	70
Syn-5H ₂ 70N ₂	0	25	5	0	70
Syn-10H ₂ 70N ₂	0	20	10	0	70
Syn-1H ₂ 60N ₂	0	39	1	0	60
Syn-1H ₂ 50N ₂	0	49	1	0	50
Syn-5H ₂ 70CO ₂	0	25	5	0	70
Syn-10H ₂ 70CO ₂	0	20	10	0	70
Syn-5H ₂ 60CO ₂	0	35	5	0	60
Syn-1H ₂ 60CO ₂	0	39	1	0	60
Syn-1H ₂ 50CO ₂	0	49	1	0	50

287 Air is supplied to the combustion chamber from a compressor. Four inlets
288 at the bottom of the settling chamber are used for maintaining a uniform flow
289 distribution at the flow straighteners entry. CO oxidation takes place by two
290 pathways namely, (1) direct oxidation ($\text{CO} + \text{O} \leftrightarrow \text{CO}_2$, $\text{CO} + \text{O} + \text{M} \leftrightarrow$
291 $\text{CO}_2 + \text{M}$) and (2) hydroxyl oxidation ($\text{CO} + \text{OH} \leftrightarrow \text{CO}_2 + \text{H}$). For pure CO
292 flames, the hydroxyl oxidation pathway is very sensitive to moisture content
293 present in the oxidizer, hence accurate determination of moisture is required.
294 Moisture filter was used to remove water vapor from the air and a humidity
295 sensor was used to measure water vapor content. It was found that water vapor
296 volume fraction does not exceed 1 %. Temperature of fuel gas issuing out of the

297 porous cylinder is measured using a K-type thermocouple (0.25 mm bead size).
298 This was required to quantify the effect of fuel heating due to the flame (details
299 discussed in section 2.1). Temperature data were recorded using the computer
300 interfaced data logger at a frequency of 2 Hz. The flame images and videos were
301 recorded using a digital camera; the lens was placed at a distance of 40 cm from
302 the combustion chamber aligned with the quartz windows.

303 *2.1. Experimental procedure*

304 As heating of porous cylinder affects the a_g values, experiments were per-
305 formed in two ways - (1) global extinction strain rate (a_g) measurement for
306 steady inlet fuel temperature issuing from porous cylinder termed as M1 or
307 method 1 and, (2) global extinction strain rate (a_g) measurement with minimal
308 inlet fuel heating termed as M2 or method 2. The experimental procedure to
309 measure a_g to quantify these effects is given below. For a particular fuel-oxidizer
310 combination, experiments were repeated at least five times (maximum deviation
311 was $< 5\%$ of the average value of a_g). Uncertainty in the measurement of a_g
312 values is equal to 1% of full-scale reading of mass flow controller used for oxi-
313 dizer flow rate measurement. Range of mass flow controller used for measuring
314 the oxidizer flow rate is 0-1000 lpm. For this range, uncertainties in the mea-
315 surement of a_g values are 17, 12, 8 and 6 s^{-1} for 10.6, 15.6, 22.8 and 30.8 mm
316 porous burner diameter respectively.

317 To measure a_g using Method 1 (M1), a stable flame was established around
318 the porous cylinder burner and fuel inlet pipe at low strain rate. The location of
319 flame was maintained sufficiently far ($\approx 20\text{--}25\text{ mm}$) to avoid direct heat transfer
320 from the flame surface to the porous cylinder fuel inlet. An oxidizer flow rate
321 of 50 lpm which corresponds to oxidizer free stream velocity of 0.23 m/s (equal
322 to 30 s^{-1} for 3.08 cm porous burner diameter) and fuel velocity of 0.33 m/s
323 was found to be suitable for avoiding heat loss by flames to the porous burner.
324 However, as the fuel was discharged only from the porous area of the burner
325 ($\pi/3$ degrees on either side of the stagnation point), heat transfer from the flame
326 to the non-porous side of burner causes an increase in fuel temperature from

327 300 K to a steady value. This steady temperature value is dependent on the
328 type of fuel and diluent used (for instance, 490 K for CH₄-70N₂ for 3.08 cm
329 porous burner diameter). Steady-state temperature increases with the decrease
330 in N₂ percentage in the fuel-inert mixture. Due to this, extinction of other three
331 CH₄-N₂ mixture used for this study occurs at higher airflow rates, which was
332 beyond the available compressor capacity (maximum flow rate the compressor
333 can supply is 650 lpm, which corresponds to 390 s⁻¹ for porous burner of di-
334 ameter of 3.08 cm). So, using method 1 (M1) extinction cannot be achieved
335 for the other three CH₄-N₂ and some syngas mixtures. Hence, experiments
336 using method 1 (M1) were performed only for the compositions (CH₄- 70N₂,
337 Syn-1H₂70N₂, Syn-5H₂70N₂, Syn-5H₂80N₂, Syn-10H₂80N₂) which are under
338 the range of compressor capacity (refer to Tables A.4 and A.5 of Appendix A
339 for data).

340 Once the fuel inlet temperature reaches a steady value, airflow rate was
341 increased to achieve extinction. With the increase in oxidizer flow rate the
342 burner temperature increases, however, difference in fuel inlet temperature from
343 the start till flame extinction was about 10-15 K. This shows that there was
344 minimal direct heat transfer from the flame surface to the fuel inlet once steady
345 state was reached and flame extinction occurs when the mixing time for fuel
346 and oxidizer becomes comparable to reaction time.

347 Figure 3 shows non-premixed flames stabilized over the porous cylinder
348 burner of diameter 3.08 cm for CH₄-70N₂-air combination obtained using M1.
349 In the figure shown, as we move from left to right, airflow rate increases causing
350 the flame to move closer to the porous burner until extinction occurs. At this
351 moment, the measured air flow rate was recorded and used to calculate a_g .

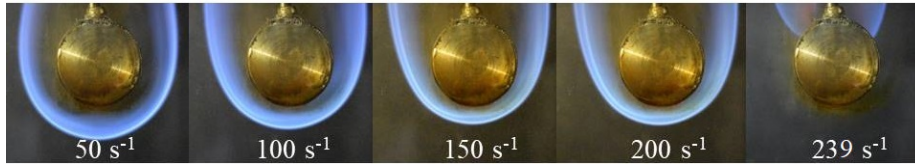


Figure 3: Combined image for Tsuji type non-premixed flames ($D = 3.08$ cm, CH_4 -70 N_2 -air combination) obtained using method 1 (M1) with increasing global strain rates until extinction

352 The other set of experiments were performed to measure the global extinc-
 353 tion strain rate with minimal heating of inlet fuel termed as M2 or method 2.
 354 Initially, at low strain rate, a stable flame was established around the burner.
 355 Once the stable flame was established, the oxidizer flow was increased (≈ 75 -
 356 $100 \text{ s}^{-1}/\text{s}$) until extinction. At this moment, flow rate and temperature were
 357 recorded. Immediately after extinction, fuel temperature was found to be in
 358 the range of 305–340 K. To minimize the effect of heating after each reading,
 359 both the combustion chamber and porous cylinder were cooled down to room
 360 temperature. Once cooled down to room temperature, the experiment was re-
 361 peated for a new reading (refer to Tables A.4, A.5, A.6 A.7, A.8, A.9, A.10 and
 362 A.11 of Appendix A for data). The a_g values obtained from M1 (steady fuel
 363 inlet temperature) is 40–60 % higher when compared to M2 (minimal heating
 364 case). The a_g data from the past literature is compared with a_g data from the
 365 M2 (see Table 3). This is due to the fact that, a_g data obtained using method 2
 366 (M2) is with minimal heating effects, which is the case with most data available
 367 from the past literature ([25, 28, 30, 31, 57]).

368 Table 3 shows the compiled data for a_g and its variation with respect to D
 369 from literature and current work. Tsuji and co-workers have performed experi-
 370 ments on three fuel-air combinations namely, CH_4 -air, C_3H_8 -air and citygas-air
 371 ([25]).

Table 3: Summary of the a_g (s^{-1}) for Tsuji type configuration

Fuel-oxidizer	D (mm)	Experiments a_g (s^{-1})	1D computation a_g (s^{-1})
Tsuji and coworkers			
CH ₄ -air	60, 15	320, 375 [25, 31]	460, 320, 350, 400-405 [28, 57]
C ₃ H ₈ -air	60, 45,	365, 420[30]	-
	30, 15	486, 650[30]	-
Ali and Varunkumar [58]			
CH ₄ -50N ₂ -air	30, 15	210, 350	-
CH ₄ -70N ₂ -air	60, 45	85, 100	-
	30, 15	120, 190	-
Current work			
CH ₄ -70N ₂ -air	30.8, 22.8	170, 211	-
	15.6, 10.6	244, 276	-
CH ₄ -N ₂ -air	30.8, 22.8	277, 349	-
	15.6, 10.6	443, 515	-
CH ₄ -30N ₂ -air	30.8, 22.8	351, 429	-
	15.6, 10.6	539, 620	-
CH ₄ -air	30.8, 22.8	380, 463	-
	15.6, 10.6	614, 756	-

372 Tsuji and co-workers have performed extensive studies on Tsuji-type con-
 373 figuration, but the only systematic study on variation of a_g with porous burner
 374 diameter (D) the authors came across is for C₃H₈-air combination ([30]). From
 375 the data shown in Table 3, it is clear that a_g decreases with increase in D .
 376 This decreasing trend for a_g is also verified by Ali and Varunkumar [58] for
 377 CH₄-70N₂-air and CH₄-50N₂-air combinations and also from the current ex-
 378 periments (see Fig. 4).

379 Figure 4 shows the a_g values for four different CH₄-N₂-air combinations
 380 from the current work. The a_g data from the current experiments show that if

381 D is decreased from 30.8 to 10.6 mm, the values of a_g increases approximately
 382 by a factor of 2.

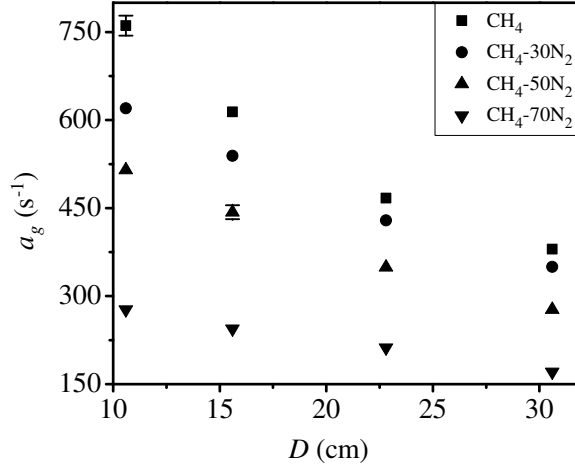


Figure 4: Variation of experimentally obtained a_g with D for four CH₄-N₂-air combinations.
 Note: Error bars less than symbol size are eliminated

383 This observation is consistent with data from Tsuji and Yamaoka [30] for
 384 C₃H₈-air. However, a_g data obtained by Tsuji and Yamaoka [31] and Tsuji
 385 [25] for CH₄-air combination do not show a significant increase in a_g with the
 386 same decrease in D . Analysis of Tsuji and Yamaoka [31] and Tsuji [25] data
 387 for CH₄-air combination shows that, as D is reduced 4 times (6 cm to 1.5 cm),
 388 a_g increases only by 17 %. This increase in a_g with decrease in D for CH₄-air
 389 combination is inconsistent with data from current work and that for C₃H₈-air
 390 a_g data (increase by factor of 2) from Tsuji and Yamaoka [30]; hence data for
 391 CH₄-air from Tsuji and Yamaoka [31] is not used for the current analysis. The
 392 reason for 15–20 % increase in the current a_g values compared to data reported
 393 in Ali and Varunkumar [58] is the reduction in non-uniformity in upstream flow
 394 in the current experimental setup.

395 As reported by Kee et al. [49], Sarnacki et al. [59] and Wang et al. [46], one of
 396 the main reasons for difference in a_g between experiments and 1D computation

397 in opposed jet configuration is due to failure of plug flow boundary condition.
 398 The porous cylinder was kept at three different values (12 cm, 10 cm and 6 cm)
 399 from the oxidizer inlet and a_g experiments were repeated using method 2 (M2)
 400 for validating the plug flow condition in Tsuji burner.

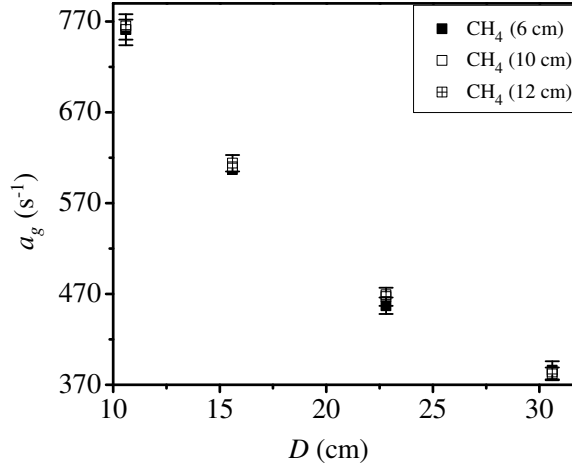


Figure 5: Variation of experimentally obtained a_g with D for CH₄-air combinations for three porous cylinder location

401 The data showed that the measured values of a_g for three distances are
 402 within 10 s^{-1} which corresponds to $\pm 3 \%$ of average a_g (refer to Table A.8
 403 of Appendix A for data). Hence, for the Tsuji type configuration, plug flow
 404 boundary condition is valid for the conditions investigated in the current work.
 405 The other two effects which can also modify the flame surface are, (1) flow-field
 406 modification by the blocking effect of a porous burner and (2) heat loss by the
 407 flame surface to the adjacent walls. To find the effect of flow-field modification
 408 by burner blocking on a_g , the wire meshes covering from the side walls were
 409 removed and experiments were repeated. The data show slightly higher a_g
 410 values for the removed wall case, but the maximum difference was 11 s^{-1} . This
 411 largest deviation in the a_g was less than 3% ($< 3 \%$) of the measured value
 412 (refer to Table A.9 of Appendix A for data).

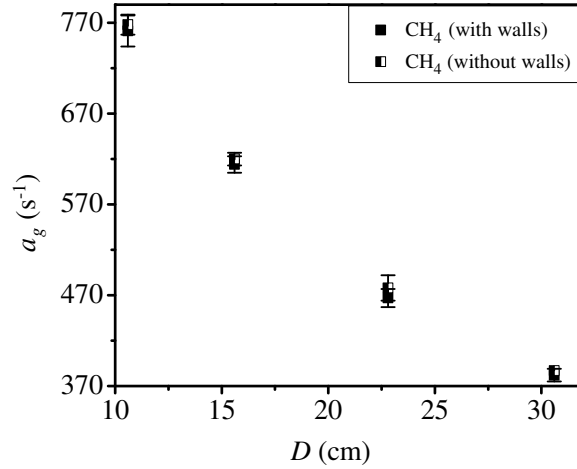


Figure 6: Variation of experimentally obtained a_g with D for CH₄-air combinations with and without side mesh walls

413 The largest porous cylinder diameter is one-fourth ($1/4$) of the combustion
 414 chamber width; this suggests that the flow blocking effect can be neglected for
 415 the porous cylinder diameters used in the current work. To find the effect of heat
 416 loss by the flame to adjacent walls on a_g , experiments are performed by cov-
 417 ering the burner casing with a thick cerawool insulation and these results were
 418 compared with experiments without insulation. Figure 7 shows the comparison
 419 of a_g values for Syn-10H₂80N₂-air combinations with and without insulation
 420 using method 2 (M2).

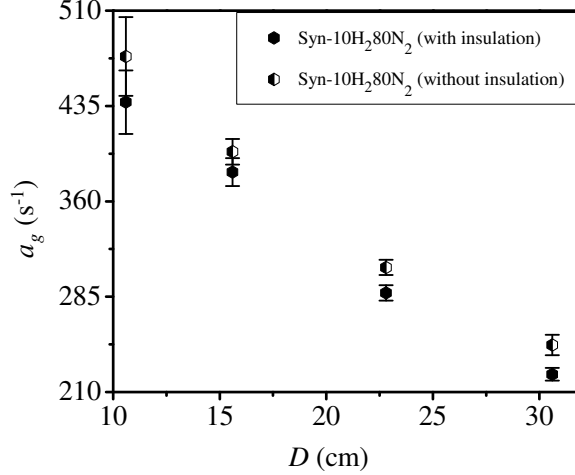


Figure 7: Variation of experimentally obtained a_g with D for Syn-10H₂80CO₂-air combinations with and without insulation using method 2 (M2)

421 The data show that, a_g values obtained using insulated burner are about
 422 16–36 s⁻¹ higher compared to non-insulated burner (refer to Table A.10 in Ap-
 423 pendix A for data). This correspond to 4-9 % of average a_g for Syn-10H₂80N₂-
 424 air combination. So, while comparing with computations for Tsuji-type config-
 425 uration, we can say a maximum of 10 % decrease in a_g can be explained through
 426 heat loss by flame.

427 3. Results and discussion

428 This section presents the results and discussion on the effect of porous cylin-
 429 der diameter (D), diluent fraction of species (CO₂ and N₂) in fuel and CO/H₂
 430 ratio on experimentally determined values of a_g .

431 3.1. Effect of porous burner diameter (D)

432 Figure 8 shows the variation of a_g values with D obtained using Method 1
 433 (M1) for CH₄ and two CO/H₂ mixtures diluted with 70 % of N₂. The data show
 434 that, a_g decreases with increase in D for all three fuel-oxidizer combinations.

435 Figure 8 shows that, a_g increases by a factor of 1.7–1.8 with decrease in porous
 436 cylinder diameter (D) from 30.8 to 10.6 mm. This increasing trend is also con-
 437 sistent with a_g data for syngas-air and $\text{CH}_4\text{-N}_2\text{-air}$ combinations obtained using
 438 M2 (see Figs. 4 and 9). The data also shows that, the fuel inlet temperature for
 439 $\text{CH}_4\text{-70N}_2$ mixture is higher in comparison to $\text{Syn-1H}_2\text{70N}_2$ and $\text{Syn-5H}_2\text{70N}_2$
 440 mixtures due to overall higher integrated heat release.

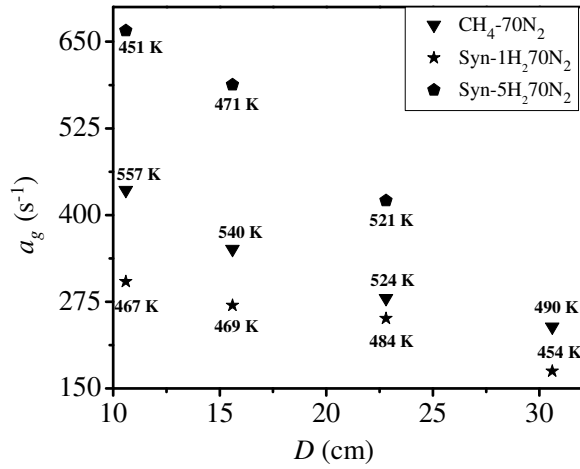
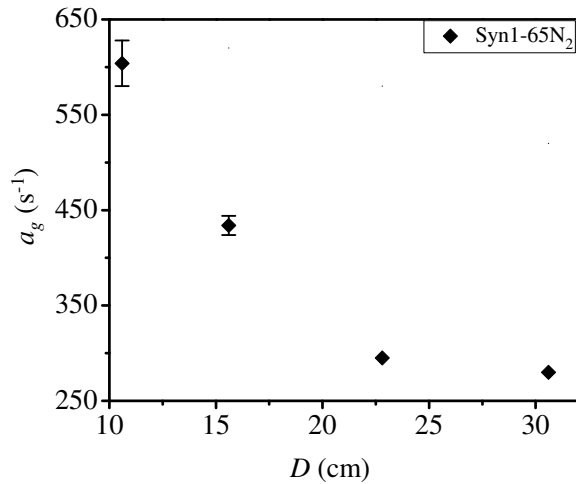


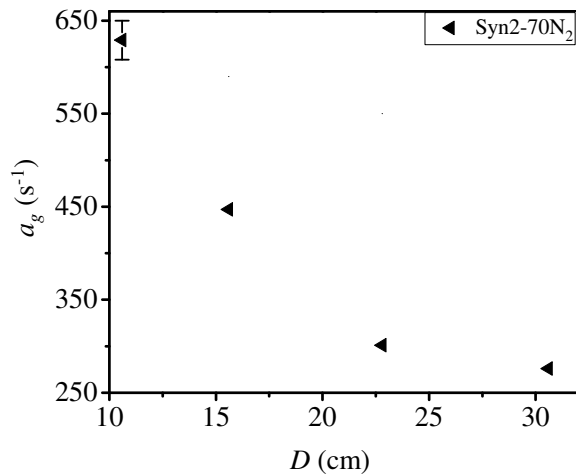
Figure 8: Variation of experimental a_g data with D obtained using Method 1 (M1) for syngas-air and methane/nitrogen-air combinations. Error bars are removed for clarity

441 The values of a_g obtained for $\text{CH}_4\text{-70N}_2$ is in between $\text{Syn-1H}_2\text{70N}_2$ and
 442 $\text{Syn-5H}_2\text{70N}_2$ mixtures. This implies that, compared to $\text{CH}_4\text{-70N}_2\text{-air}$ the over-
 443 all reactivity of $\text{Syn-1H}_2\text{70N}_2\text{-air}$ is lower and $\text{Syn-5H}_2\text{70N}_2\text{-air}$ is higher for the
 444 same percentage of diluent in the fuel (70 % N_2 v/v). Wang et al. [46] have
 445 obtained a_g data for opposed jet non-premixed syngas flames for a wide range
 446 of compositions; comparisons have also been drawn with results from 2D axi-
 447 symmetric computations from their study. In the current study, we have chosen
 448 two compositions from Wang et al. [46] (referred to here as Syn2-70N_2 and
 449 Syn1-65N_2 , see Table 2 for details) to measure a_g using Tsuji burner.

450 Figures 9a and 9b show the variation of experimentally obtained a_g with
451 D for Syn1-65N₂-air and Syn2-70N₂-air compositions using method 2 (M2).
452 The data show that, with decrease in D from 30.8 to 10.6 mm a_g increases
453 by a factor of 2.15-2.25. For Syn1-65N₂-air combination, a_g value obtained
454 experimentally using Tsuji burner (604 ± 24 s⁻¹) for 10.6 mm diameter is close
455 to a_g value (647 ± 70 s⁻¹) obtained by Wang et al. [46] for a uniform velocity
456 profile for nozzle separation distance of 10.2 mm. For parabolic velocity pro-
457 file, for the same composition experimental obtained a_g value (311 ± 50 s⁻¹) by
458 Wang et al. [46] is close to a_g value (295 ± 9 s⁻¹) obtained using Tsuji burner
459 of 22.8 mm diameter. Understanding the connections between the extinction
460 strain rates obtained from different configurations and its interpretation for the
461 optimization/validation of kinetic mechanisms require further experimental and
462 computational studies.



(a) CO/H₂ = 2 (35 % by volume)



(b) CO/H₂ = 1 (30 % by volume)

Figure 9: Experimentally obtained a_g values for Syn1-65N₂ and Syn2-70N₂ using method 2 (M2) for Tsuji type configuration

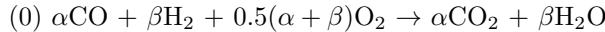
463 The analysis of computational and experimental data from Wang et al. [46]
 464 for these two compositions (Syn1-65N₂ and Syn2-30N₂) show that, 2D axi-

465 symmetric computations under predict a_g by at least 50 % of experimentally
 466 obtained values (see Table A.4 in Appendix A for data). They have proposed
 467 that the possible reason for this under-prediction is failure of the assumption
 468 of top-hat/parabolic velocity profiles at the nozzles exit. The experiments per-
 469 formed in the current study using Tsuji type configuration have shown that the
 470 flow field around the flame is not modified by the oxidizer boundary if the dis-
 471 tance between the porous burner and oxidizer inlet is greater than 2 times the
 472 largest burner diameter (D) (see Fig. 5). Hence, experimental a_g data obtained
 473 using Tsuji-type configuration is perhaps better suited for predicting extinction
 474 using 2D planar computation without concerning about the validity of boundary
 475 conditions.

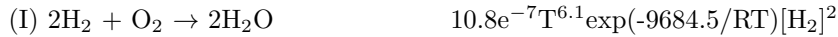
476 3.2. Effect of diluent on a_g - N_2 vs CO_2

477 Figures 10a and 10b show the comparison of a_g values obtained by method
 478 2 (M2) using two different CO/H₂ ratios (5 and 2) for a fixed diluent percentage.
 479 The data show that for all porous burner diameters (D) and CO/H₂ ratio used,
 480 a_g values obtained using N₂ as diluent are always 1.6–2.25 times the a_g values
 481 obtained using CO₂ as diluent. To explain this difference in a_g values, an overall
 482 reaction rate (ω_o) is calculated using a two step kinetic mechanism proposed by
 483 Slavinskaya et al. [60].

Overall reaction



Slavinskaya two-step mechanism



484 For the given two-step kinetic mechanism, H₂ and CO consumption rates
 485 are $\omega_{H_2} = 2\omega_I + \omega_{II}$ and $\omega_{CO} = \omega_{II}$, where ω_I and ω_{II} are the rates of these
 486 two reactions. The units used for the kinetic mechanism are: mole, cm³, sec, K
 487 and cal. In the overall reaction, α and β are the volumetric fractions of CO and

488 H₂ present in the fuel. The overall reaction rate is calculated by equating the
 489 heat release rate of Slavinskaya et al. [60] mechanism with an overall reaction.

$$\omega_o = \frac{2\omega_I(h_{f,H_2O}^o) + \omega_{II}(h_{f,CO_2}^o + h_{f,H_2O}^o - h_{f,CO}^o)}{\beta(h_{f,H_2O}^o) + \alpha(h_{f,CO_2}^o - h_{f,CO}^o)} \quad (2)$$

490 In the Eqn 2, h_{f,H_2O}^o , h_{f,CO_2}^o and $h_{f,CO}^o$ are standard heat of formation of H₂O,
 491 CO₂ and CO. The reaction rates ω_I and ω_{II} are given by Eqns. 3 and 4 when
 492 expressed in terms of mole fractions (X_{H_2} , X_{CO_2} and X_{H_2O}), pressure (P) and
 493 temperature (T).

$$\omega_I = 10.8e^{-7T^{6.1}} \exp\left(\frac{-9684.5}{RT}\right) \left(\frac{P}{R_u T} X_{H_2}\right)^2 \left(\frac{mole}{cm^3 s}\right) \quad (3)$$

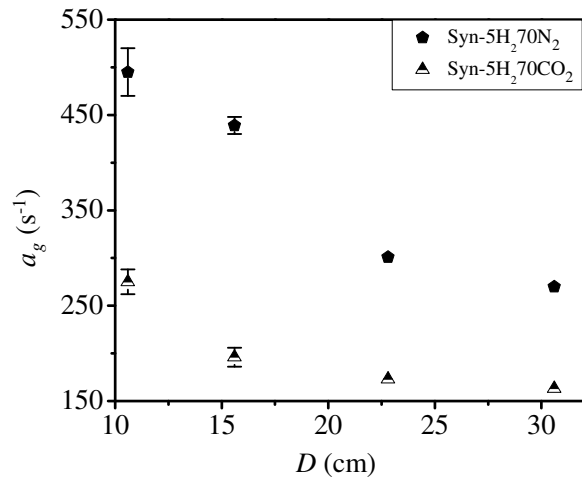
$$\omega_{II} = 20.15e^{-8T^{5.9}} \exp\left(\frac{-6097.6}{RT}\right) \left(\frac{P}{R_u T}\right)^{2.4} X_{O_2} (X_{CO})^{1.4} \left(\frac{mole}{cm^3 s}\right) \quad (4)$$

$$X_{H_2} = \frac{\beta}{1 + [2.38(\alpha + \beta)]/\phi} \quad (5)$$

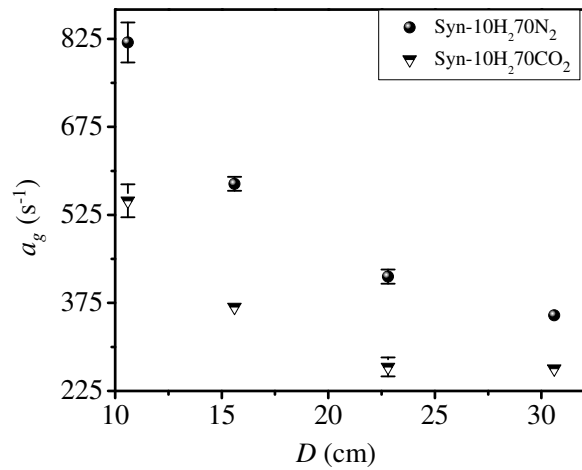
$$X_{CO} = \frac{\alpha}{1 + [2.38(\alpha + \beta)]/\phi} \quad (6)$$

$$X_{O_2} = \frac{(\alpha + \beta)/2\phi}{1 + [2.38(\alpha + \beta)]/\phi} \quad (7)$$

498 where, α , β represents volumetric percentage of CO and H₂ in fuel and ϕ repre-
 499 sents the equivalence ratio. The location of the non-premixed flame is assumed
 500 at $\phi = 1$. The equilibrium temperature obtained for Syn-5H₂70N₂-air and
 501 Syn-5H₂70CO₂-air combinations using NASA SP-273 software ([61]) for con-
 502 stant pressure condition is 1760 K and 1500 K respectively. With the increase
 503 in flame temperature from 1500 to 1760 K, the rate of two reactions (ω_I and
 504 ω_{II}) increases by factor of 3.3 and 2.4 respectively. The overall reaction rate
 505 (ω_o) of the mixture with N₂ is more than that of the one with CO₂ by a factor
 506 of 3.1. This is consistent with the observed differences in the global strain rate.



(a) $CO/H_2 = 5$ (30 % by volume)

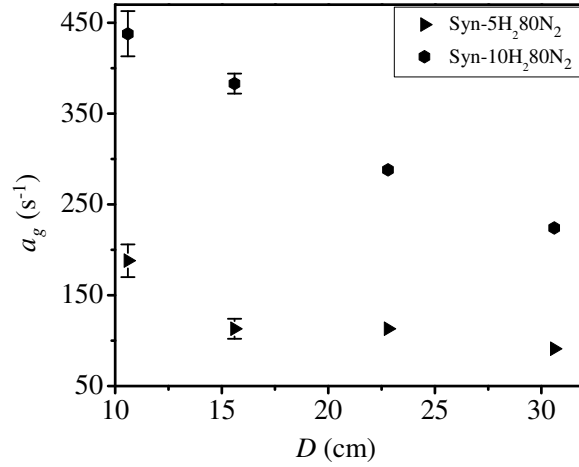


(b) $CO/H_2 = 2$ (30 % by volume)

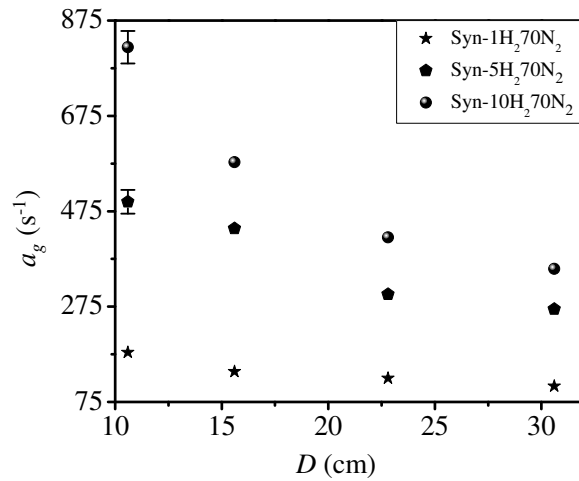
Figure 10: Comparison of experimentally obtained a_g using method 2 (M2) diluted with N₂ and CO₂ for different D values

507 *3.3. Effect of H₂ and CO % in fuel*

508 Figures 11a and 11b show the effect of volumetric H₂ % on a_g values ob-
509 tained by Method 2 (M2) using N₂ as diluent (70 % and 80 % by volume). The
510 data show that, a_g increases approximately 1.3–1.7 times when volumetric H₂
511 % is increased from 5 to 10 % for 70 % N₂ (v/v) in fuel mixture. However, a_g
512 increases by 2.5–3.8 times approximately, if the volumetric H₂ % is increased
513 from 1 to 5 %. Extinction strain rate (a_g) increases by 3–3.8 times approxi-
514 mately, if the volumetric H₂ % is increased from 5 to 10 % for 80 % N₂ (v/v) in
515 fuel mixture. The ratios of overall reaction rates (ω_o) calculated using Eqn. 2
516 for compositions Syn-5H₂70N₂/Syn-1H₂70N₂ and Syn-10H₂70N₂/Syn-5H₂70N₂
517 are 10.4 and 3.6. This shows that, a_g increases non-linearly ($\approx \sqrt{\omega_o}$) with in-
518 crease in overall reactivity. For both H₂ and CO, hydroxyl pathway (CO + OH
519 \leftrightarrow CO₂ + H, H₂ + OH \leftrightarrow H₂O + H) is dominant for oxidation. Shih and Hsu
520 [34] have shown that OH radicals are produced mainly by two reactions which
521 are H + O₂ \leftrightarrow O + OH and O + H₂O \leftrightarrow OH + OH. The equilibrium temper-
522 ature calculated for the three compositions (Syn-1H₂70N₂, Syn-5H₂70N₂ and
523 Syn-10H₂70N₂) is 1775, 1760 and 1741 K respectively. The data show that the
524 flame temperature does not vary significantly with increase in H₂ % in fuel. For
525 these conditions, the rate constant of hydroxyl oxidation pathways of CO and
526 H₂ remains approximately same. Hence, the overall reaction rate is predom-
527 inantly limited by amount of OH radical produced during the reaction. Shih
528 and Hsu [34] computational study shows that for very small H₂ % in syngas
529 mixtures the overall reactivity of mixture is governed by CO hydroxyl oxidation
530 path (CO + H₂ \leftrightarrow CO₂ + H). With increase in H₂ % the overall reactivity of
531 mixture shifts towards H₂ oxidation by reaction OH + H₂ \leftrightarrow H₂O + H ([34]). It
532 is possible that the OH radical concentration increases at much faster rate with
533 1 to 5 % increase H₂ in comparison to 5 to 10 % of H₂ in the fuel mixture. This
534 can be a possible reason to explain the non-linear increase in a_g with increase
535 in H₂ %. Computations are needed to be performed to explore this further.



(a) (CO + H₂) = 20 % by volume



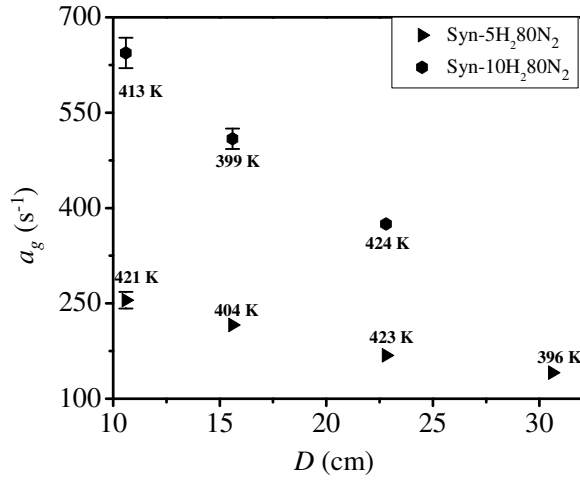
(b) (CO + H₂) = 30 % by volume

Figure 11: Effect of H₂ percentage on experimentally obtained a_g using method 2 (M2) diluted with N₂

536 The effect of volumetric H₂ % on a_g values is also studied using M1. Fig-
 537 ure 12 shows the comparison of a_g and respective inlet fuel temperature at

538 extinction for two H₂ (5 and 10 % by volume) fraction in fuel with 80 % N₂. It
 539 was observed that the inlet fuel temperature remain more or less the same with
 540 change in H₂ percentage, but a_g increases by factor 2–2.5.

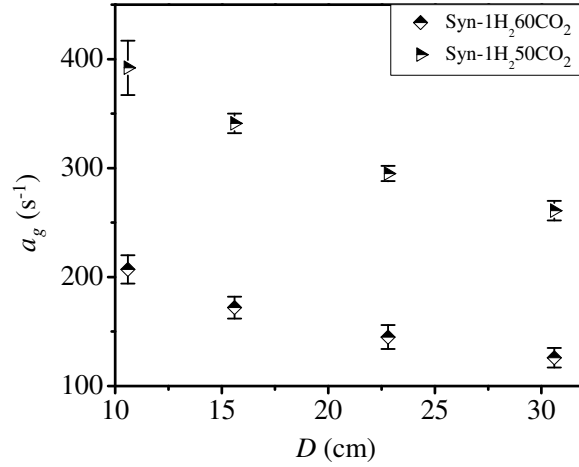
541 The next set of a_g data is generated for fuel having very high CO/H₂ ratio.
 542 This dataset is useful for validation of kinetic parameters for direct (CO + O
 543 \rightleftharpoons CO₂, CO + O + M \rightleftharpoons CO₂ + M) and hydroxyl oxidation pathways (CO +
 544 OH \rightleftharpoons CO₂ + H) for CO oxidation for any given kinetic mechanism.



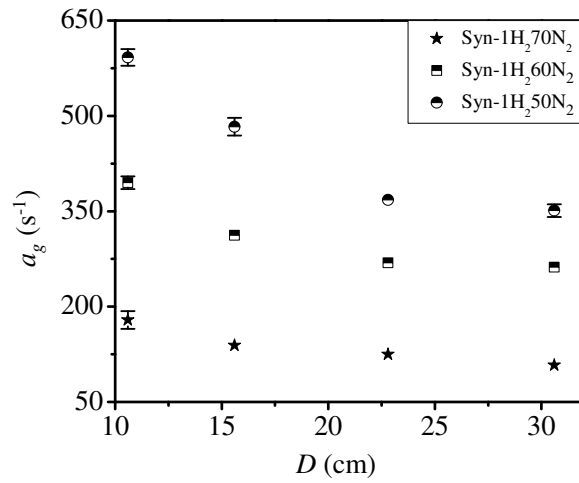
(a) (CO + H₂) = 20 % by volume

Figure 12: Variation of experimental a_g data with D obtained using method 1 (M1) for syngas-air and methane/nitrogen-air combinations

545 Figures 13a and 13b show the comparison of experimentally obtained a_g
 546 using method 2 (M2) for high CO flames diluted with N₂ and CO₂. The data
 547 show that, irrespective of CO₂ or N₂ used as diluent, a_g increases by factor
 548 of 2–2.5 with 10 % increase in CO. This ratio decreases to 1.5–1.7 with 10 %
 549 decrease in diluent for Syn-1H₂60N₂-air combination.



(a) High CO flames with CO₂ as diluent

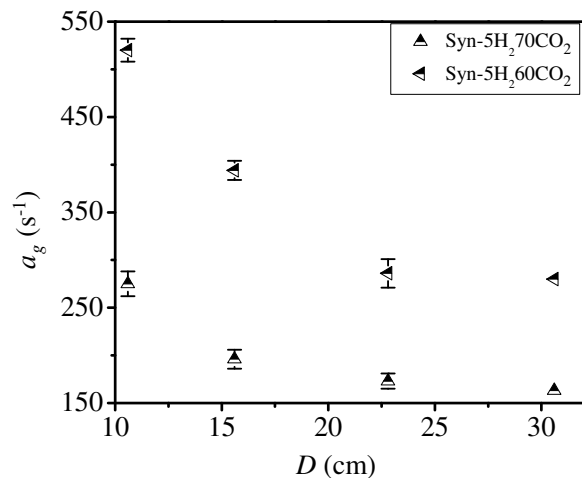


(b) High CO flames with N₂ as diluent

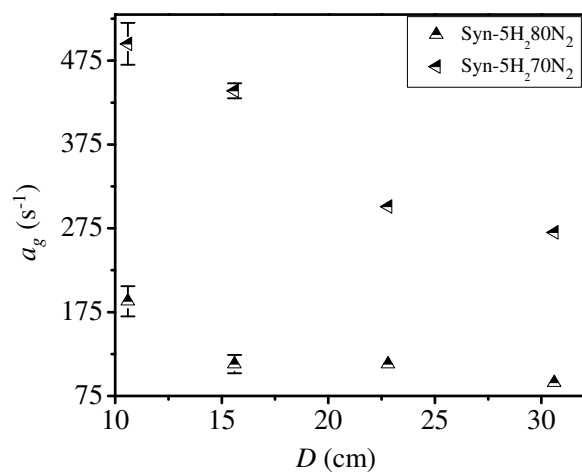
Figure 13: Comparison of experimentally obtained a_g for High CO flames diluted with N₂ and CO₂

550 Experiments performed using 5 % H₂ by volume also show the same percent-
 551 age increase in a_g values. Figures 14a and 14b show that, a_g values increases by

552 factor of 2–2.5 times for CO₂ and 2.6–3.8 times for N₂ with 10 % increase in CO
553 by volume in fuel mixtures containing 5 % H₂. Higher CO % in the fuel gives
554 higher flame temperature which increases the overall fuel reactivity leading to
555 increase in a_g values.



(a) 5 % H₂ by volume with CO₂ as diluent



(b) 5 % H₂ by volume with N₂ as diluent

Figure 14: Comparison of experimentally obtained a_g for difference CO % diluted with N₂ and CO₂

556 The ratios of overall reaction rates (ω_o) calculated using Eqn. 2 for composi-
 557 tions Syn-1H₂60N₂/Syn-1H₂70N₂ and Syn-1H₂50N₂/Syn-1H₂60N₂ are 1.6 and

558 1.3 respectively. For the same case, the ratio of experimentally obtained a_g val-
559 ues are 2.1–2.4 and 1.5–1.7 respectively. Hydroxyl radical (OH) concentration
560 in mixture depends on H₂ % in the fuel and flame temperature. The data shows
561 that, equilibrium temperature increases with increase in CO % in the fuel (1775,
562 1973 and 2106 K for Syn-1H₂70N₂, Syn-1H₂60N₂ and Syn-1H₂50N₂). Hence, it
563 is possible for a fixed H₂ % in fuel OH concentration reduces with in increase
564 in CO % leading to reduction in a_g ratio.

565 4. Conclusion and future Work

566 In the present study, global extinction strain rate (a_g) is obtained for CH₄/N₂-
567 air and syngas-air non-premixed flame using Tsuji-type counterflow configura-
568 tion. The effect of porous burner diameter (D) on a_g value, that is, a_g decrease
569 with increase in D is determined. Plug flow boundary condition is experimen-
570 tally verified by obtaining a_g at three distances of oxidizer inlet from the porous
571 burner. The flow-field blocking by porous burner has shown a deviation of less
572 than 3 % in a_g for a CH₄-air combination. Hence, the blocking effect of burner
573 diameter (D) of dimensions less than 1/4 of combustion chamber side wall length
574 is negligible. The past literature shows the failure of assumed velocity profiles
575 at the nozzle exit as the possible reason for under-prediction of a_g for opposed
576 jet counterflow configuration. This issue can be resolved by using Tsuji type
577 configuration for extinction studies. Convective and radiative heat loss by the
578 flame to ambient can cause 4–9 % decrease in a_g values. So, for accurate a_g
579 predictions these losses should be incorporated in 2D planar simulations. Ni-
580 trogen when used as a diluent, yields 1.6–2.25 times higher a_g in comparison
581 to CO₂ used as diluent. Increasing H₂ from 1 to 5 % leads to 2.5–3.8 times
582 increase in a_g compared to 1.3–1.7 times increase in a_g with 5 to 10 % increase
583 in H₂ for fuel mixture consisting of 70 % N₂ by volume. Increasing CO by
584 10 % leads to 1.5–2.4 times increase in a_g for fuel mixtures consisting of H₂
585 (1 and 5 % by v/v), CO₂ (50, 60 and 70 % by v/v) and N₂ (50, 60, 70 and
586 80 % by v/v). The comparison of overall reactivity (ω_o) with a_g shows that,

587 a_g increase non-linearly ($\approx \sqrt{w_o}$) with increase in H₂ % in fuel mixture. This
588 increase in a_g with an increase H₂ % in fuel mixture can be explained from
589 the OH radical concentration which requires 2D computations using simplified
590 kinetic mechanism and will be taken up in future.

591 **Acknowledgements**

592 We are thankful to Ms. Kathyayani. N for providing technical assistance in
593 conducting experiments. We are also thankful to Dr. Faheem Ulla Khan for
594 constructive criticism on the manuscript.

595 **Nomenclature**

596 α	CO % in fuel (v/v)
597 β	H ₂ % in fuel (v/v)
598 ω_I	Reaction rate 1 (mole/cm ³ s)
599 ω_{II}	Reaction rate 2 (mole/cm ³ s)
600 ω_{CO}	Overall CO consumption rate (mole/cm ³ s)
601 ω_{H_2}	Overall H ₂ consumption rate (mole/cm ³ s)
602 ω_o	Overall fuel consumption rate (mole/cm ³ s)
603 ϕ	Equivalence ratio
604 a_g	Global extinction strain rate (s ⁻¹)
605 D	Porous cylinder radius (m)
606 du/dx	axial velocity gradient (s ⁻¹)
607 h	Combustion chamber height (m)
608 h_{f,CO_2}^o	Heat of formation of CO ₂ (KJ/mol-K)

609	$h_{f,CO}^o$	Heat of formation of CO (KJ/mol-K)
610	h_{f,H_2O}^o	Heat of formation of H ₂ O (KJ/mol-K)
611	l	Combustion chamber length (m)
612	u_{ox}	free stream oxidizer velocity (m/s)
613	w	Combustion chamber width (m)
614	a_l	Local extinction strain rate (s ⁻¹)
615	P	Pressure (N/m ²)
616	P	Temperature (K)
617	X_{CO}	Mole fraction of CO
618	X_{H_2}	Mole fraction of H ₂
619	X_{O_2}	Mole fraction of O ₂

620

621 **References**

- 622 [1] V. Jaganathan, S. Varunkumar, Net carbon-di-oxide conversion and other
623 novel features of packed bed biomass gasification with o₂/co₂ mixtures,
624 Fuel 244 (2019) 545–558.
- 625 [2] V. Jaganathan, O. Mohan, S. Varunkumar, Intrinsic hydrogen yield from
626 gasification of biomass with oxy-steam mixtures, International Journal of
627 Hydrogen Energy (2019).
- 628 [3] N. Gnanapragasam, M. Rosen, A review of hydrogen production using
629 coal, biomass and other solid fuels, Biofuels 8 (2017) 725–745.
- 630 [4] M. M. Joshi, S. Lee, Integrated gasification combined cyclea review of igcc
631 technology, Energy Sources 18 (1996) 537–568.

- 632 [5] D. Sanchez, R. Chacartegui, J. Munoz, A. Munoz, T. Sanchez, Performance
633 analysis of a heavy duty combined cycle power plant burning various syngas
634 fuels, *International Journal of Hydrogen Energy* 35 (2010) 337–345.
- 635 [6] A. L. Boehman, O. L. Corre, Combustion of syngas in internal combustion
636 engines, *Combustion science and technology* 180 (2008) 1193–1206.
- 637 [7] S. Verhelst, Recent progress in the use of hydrogen as a fuel for internal
638 combustion engines, *international journal of hydrogen energy* 39 (2014)
639 1071–1085.
- 640 [8] M. Klell, H. Eichseder, M. Sartory, Mixtures of hydrogen and methane in
641 the internal combustion engine–synergies, potential and regulations, *Inter-
642 national journal of hydrogen energy* 37 (2012) 11531–11540.
- 643 [9] S. Varunkumar, N. Rajan, H. Mukunda, Single particle and packed bed
644 combustion in modern gasifier stovesdensity effects, *Combustion Science
645 and Technology* 183 (2011) 1147–1163.
- 646 [10] S. Varunkumar, N. Rajan, H. Mukunda, Experimental and computational
647 studies on a gasifier based stove, *Energy Conversion and Management* 53
648 (2012) 135–141.
- 649 [11] A. K. Das, K. Kumar, C.-J. Sung, Laminar flame speeds of moist syngas
650 mixtures, *Combustion and Flame* 158 (2011) 345–353.
- 651 [12] N. Bouvet, C. Chauveau, I. Gökalp, S.-Y. Lee, R. J. Santoro, Charac-
652 terization of syngas laminar flames using the bunsen burner configuration,
653 *International Journal of Hydrogen Energy* 36 (2011) 992–1005.
- 654 [13] H. Lee, L. Jiang, A. Mohamad, A review on the laminar flame speed and
655 ignition delay time of syngas mixtures, *International Journal of Hydrogen
656 Energy* 39 (2014) 1105–1121.
- 657 [14] O. Askari, Z. Wang, K. Vien, M. Sirio, H. Metghalchi, On the flame
658 stability and laminar burning speeds of syngas/o₂/he premixed flame, *Fuel*
659 190 (2017) 90–103.

- 660 [15] E. Monteiro, M. Bellenoue, J. Sotton, N. A. Moreira, S. Malheiro, Laminar
661 burning velocities and markstein numbers of syngas-air mixtures, *Fuel* 89
662 (2010) 1985–1991.
- 663 [16] R. J. Varghese, H. Kolekar, V. Hariharan, S. Kumar, Effect of co content
664 on laminar burning velocities of syngas-air premixed flames at elevated
665 temperatures, *Fuel* 214 (2018) 144–153.
- 666 [17] R. J. Varghese, H. Kolekar, S. Kumar, Demarcation of reaction effects
667 on laminar burning velocities of diluted syngas-air mixtures at elevated
668 temperatures, *International Journal of Chemical Kinetics* 51 (2019) 95–
669 104.
- 670 [18] R. J. Varghese, H. Kolekar, S. Kumar, Laminar burning velocities of
671 h₂/co/ch₄/co₂/n₂-air mixtures at elevated temperatures, *International*
672 *Journal of Hydrogen Energy* 44 (2019) 12188–12199.
- 673 [19] A. Cuoci, A. Frassoldati, G. B. Ferraris, T. Faravelli, E. Ranzi, The igni-
674 tion, combustion and flame structure of carbon monoxide/hydrogen mix-
675 tures. note 2: Fluid dynamics and kinetic aspects of syngas combustion,
676 *International Journal of Hydrogen Energy* 32 (2007) 3486–3500.
- 677 [20] A. Frassoldati, T. Faravelli, E. Ranzi, The ignition, combustion and flame
678 structure of carbon monoxide/hydrogen mixtures. note 1: Detailed kinetic
679 modeling of syngas combustion also in presence of nitrogen compounds,
680 *International Journal of Hydrogen Energy* 32 (2007) 3471–3485.
- 681 [21] H.-M. Li, G.-X. Li, Z.-Y. Sun, Y. Zhai, Z.-H. Zhou, Measurement of the
682 laminar burning velocities and markstein lengths of lean and stoichiometric
683 syngas premixed flames under various hydrogen fractions, *international*
684 *journal of hydrogen energy* 39 (2014) 17371–17380.
- 685 [22] H. A. Yepes, A. A. Amell, Laminar burning velocity with oxygen-enriched
686 air of syngas produced from biomass gasification, *International Journal of*
687 *Hydrogen Energy* 38 (2013) 7519–7527.

- 688 [23] N. Bouvet, C. Chauveau, I. Gökalp, F. Halter, Experimental studies of the
689 fundamental flame speeds of syngas (h₂/co)/air mixtures, Proceedings of
690 the Combustion Institute 33 (2011) 913–920.
- 691 [24] R. Bilger, Reaction rates in diffusion flames, Combustion and Flame 30
692 (1977) 277–284.
- 693 [25] H. Tsuji, Counterflow diffusion flames, Progress in energy and combustion
694 science 8 (1982) 93–119.
- 695 [26] R. Barlow, G. Fiechtner, C. Carter, J.-Y. Chen, Experiments on the scalar
696 structure of turbulent *co/h₂/n₂* jet flames, Combustion and Flame 120
697 (2000) 549–569.
- 698 [27] O. A. Marzouk, E. D. Huckaby, A comparative study of eight finite-rate
699 chemistry kinetics for *co/h₂* combustion, Engineering applications of com-
700 putational fluid mechanics 4 (2010) 331–356.
- 701 [28] H. Chelliah, C. Law, T. Ueda, M. Smooke, F. Williams, An experimental
702 and theoretical investigation of the dilution, pressure and flow-field effects
703 on the extinction condition of methane-air-nitrogen diffusion flames, Sym-
704 posium (International) on Combustion 23 (1991) 503–511.
- 705 [29] K. Seshadri, F. Williams, Laminar flow between parallel plates with injec-
706 tion of a reactant at high reynolds number, International Journal of Heat
707 and Mass Transfer 21 (1978) 251–253.
- 708 [30] H. Tsuji, I. Yamaoka, The counterflow diffusion flame in the forward stag-
709 nation region of a porous cylinder, Symposium (International) on Combustion
710 11 (1967) 979–984.
- 711 [31] H. Tsuji, I. Yamaoka, The structure of counterflow diffusion flames in the
712 forward stagnation region of a porous cylinder, Symposium (International)
713 on Combustion 12 (1969) 997–1005.

- 714 [32] D. E. Giles, S. Som, S. K. Aggarwal, Nox emission characteristics of coun-
715 terflow syngas diffusion flames with airstream dilution, *Fuel* 85 (2006)
716 1729–1742.
- 717 [33] A. Sahu, R. Ravikrishna, A detailed numerical study of nox kinetics in
718 low calorific value h₂/co syngas flames, *International Journal of Hydrogen*
719 *Energy* 39 (2014) 17358–17370.
- 720 [34] H.-Y. Shih, J.-R. Hsu, Computed nox emission characteristics of opposed-
721 jet syngas diffusion flames, *Combustion and Flame* 159 (2012) 1851–1863.
- 722 [35] S. Park, Y. Kim, Effects of nitrogen dilution on the nox formation char-
723 acteristics of ch₄/co/h₂ syngas counterflow non-premixed flames, *Interna-*
724 *tional Journal of Hydrogen Energy* 42 (2017) 11945–11961.
- 725 [36] D. Ning, A. Fan, H. Yao, Effect of radiation emission and reabsorption
726 on flame temperature and no formation in h₂/co/air counterflow diffusion
727 flames, *International Journal of Hydrogen Energy* 42 (2017) 22015–22026.
- 728 [37] K.-H. Yang, H.-Y. Shih, No formation of opposed-jet syngas diffusion
729 flames: Strain rate and dilution effects, *International Journal of Hydrogen*
730 *Energy* 42 (2017) 24517–24531.
- 731 [38] S. Som, A. Ramirez, J. Hagerdorn, A. Saveliev, S. Aggarwal, A numerical
732 and experimental study of counterflow syngas flames at different pressures,
733 *Fuel* 87 (2008) 319–334.
- 734 [39] J. Park, D. S. Bae, M. S. Cha, J. H. Yun, S. I. Keel, H. C. Cho, T. K. Kim,
735 J. S. Ha, Flame characteristics in h₂/co synthetic gas diffusion flames
736 diluted with co₂: effects of radiative heat loss and mixture composition,
737 *international journal of hydrogen energy* 33 (2008) 7256–7264.
- 738 [40] J. Park, O. B. Kwon, J. H. Yun, S. I. Keel, H. C. Cho, S. Kim, Preferential
739 diffusion effects on flame characteristics in h₂/co syngas diffusion flames
740 diluted with co₂, *international journal of hydrogen energy* 33 (2008) 7286–
741 7294.

- 742 [41] H.-Y. Shih, J.-R. Hsu, Dilution effects analysis of opposed-jet h₂/co syngas
743 diffusion flames, *Combustion Theory and Modelling* 17 (2013) 543–562.
- 744 [42] J. Park, J. S. Kim, J. O. Chung, J. H. Yun, S. I. Keel, Chemical effects of
745 added co₂ on the extinction characteristics of h₂/co/co₂ syngas diffusion
746 flames, *international journal of hydrogen energy* 34 (2009) 8756–8762.
- 747 [43] H.-Y. Shih, J.-R. Hsu, A computational study of combustion and extinction
748 of opposed-jet syngas diffusion flames, *international journal of hydrogen
749 energy* 36 (2011) 15868–15879.
- 750 [44] M. Safer, F. Tabet, A. Ouadha, K. Safer, A numerical investigation of
751 structure and emissions of oxygen-enriched syngas flame in counter-flow
752 configuration, *international journal of hydrogen energy* 40 (2015) 2890–
753 2898.
- 754 [45] H.-Y. Shih, J.-R. Hsu, Y.-H. Lin, Computed flammability limits of opposed-
755 jet h₂/co syngas diffusion flames, *International Journal of Hydrogen Energy*
756 39 (2014) 3459–3468.
- 757 [46] W. Wang, A. E. Karatas, C. P. Groth, Ö. L. Gülder, Experimental and
758 numerical study of laminar flame extinction for syngas and syngas-methane
759 blends, *Combustion Science and Technology* 190 (2018) 1455–1471.
- 760 [47] J. Fu, C. Tang, W. Jin, Z. Huang, Effect of preferential diffusion and flame
761 stretch on flame structure and laminar burning velocity of syngas bunsen
762 flame using oh-plif, *international journal of hydrogen energy* 39 (2014)
763 12187–12193.
- 764 [48] A. Sahu, R. Ravikrishna, Effect of h₂/co composition on extinction strain
765 rates of counterflow syngas flames, *Energy & Fuels* 29 (2015) 4586–4596.
- 766 [49] R. J. Kee, J. A. Miller, G. H. Evans, G. Dixon-Lewis, A computational
767 model of the structure and extinction of strained, opposed flow, premixed
768 methane-air flames 22 (1989) 1479–1494.

- 769 [50] J. Li, Z. Zhao, A. Kazakov, M. Chaos, F. L. Dryer, J. J. Scire Jr, A
770 comprehensive kinetic mechanism for co, ch₂o, and ch₃oh combustion, In-
771 ternational Journal of Chemical Kinetics 39 (2007) 109–136.
- 772 [51] G. Smith, D. Golden, M. Frenklach, N. Moriarty, B. Eiteneer, M. Golden-
773 berg, C. Bowman, R. Hanson, S. Song, W. Gardiner, et al., Gri-mech 3.0
774 [http://www. me. berkeley. edu/gri_mech](http://www.me.berkeley.edu/gri_mech), Last visited March (2007).
- 775 [52] S. G. Davis, A. V. Joshi, H. Wang, F. Egolfopoulos, An optimized kinetic
776 model of h₂/co combustion, Proceedings of the Combustion Institute 30
777 (2005) 1283–1292.
- 778 [53] M. A. Mueller, R. A. Yetter, F. Dryer, Flow reactor studies and kinetic
779 modeling of the h₂/o₂/nox and co/h₂o/o₂/nox reactions, International
780 Journal of Chemical Kinetics 31 (1999) 705–724.
- 781 [54] F. Dryer, I. Glassman, High-temperature oxidation of co and ch₄, Sympo-
782 sium (International) on combustion 14 (1973) 987–1003.
- 783 [55] G. Williams, H. Hottel, A. Morgan, The combustion of methane in a jet-
784 mixed reactor, in: Symposium (International) on Combustion, volume 12,
785 Elsevier, pp. 913–925.
- 786 [56] S. Varunkumar, N. Rajan, H. Mukunda, Universal flame propagation be-
787 havior in packed bed of biomass, Combustion Science and Technology 185
788 (2013) 1241–1260.
- 789 [57] G. Dixon-Lewis, T. David, P. Gaskell, S. Fukutani, H. Jinno, J. Miller,
790 R. Kee, M. Smooke, N. Peters, E. Effelsberg, et al., Calculation of the
791 structure and extinction limit of a methane-air counterflow diffusion flame
792 in the forward stagnation region of a porous cylinder, Symposium (Inter-
793 national) on Combustion 20 (1985) 1893–1904.
- 794 [58] S. M. Ali, S. Varunkumar, On the extinction strain rate of counterflow
795 diffusion flames, 11th Asia-Pacific Conference on Combustion (2017) 4.

- 796 [59] B. Sarnacki, G. Esposito, R. Krauss, H. Chelliah, Extinction limits and
797 associated uncertainties of nonpremixed counterflow flames of methane,
798 ethylene, propylene and n-butane in air, *Combustion and Flame* 159 (2012)
799 1026–1043.
- 800 [60] N. Slavinskaya, M. Braun-Unkhoff, P. Frank, Reduced reaction mechanisms
801 for methane and syngas combustion in gas turbines, *Journal of engineering*
802 for gas turbines and power 130 (2008) 021504.
- 803 [61] S. Gordon, J. McBride, Nasa sp-273, NASA Lewis Research, Cleveland,
804 OH (1976).

805 **Appendix A. Global extinction strain rate (a_g) experimental data**

Table A.4: Global extinction strain (a_g) and burner temperature (T) data for CH₄-N₂-air combinations

D (mm)	10.6	15.6	22.8	30.8
Fuel	a_g (s^{-1})/ T (K)			
M2				
CH ₄	761±17/-	614±9/-	467±10/-	380±7/-
CH ₄ -30N ₂	620±5/-	539±4/-	429±5/-	350±4/-
CH ₄ -50N ₂	515±6/-	443±12/-	349±5/-	277±4/-
CH ₄ -70N ₂	277±5/-	244±10/-	211±8/-	170±3/-
M1				
CH ₄ -70N ₂	436±5/557	351±2/540	280±3/524	239±2/490

Table A.5: Global extinction strain (a_g) and burner temperature (T) data for Syn-H₂N₂-air combinations

D (mm)	10.6	15.6	22.8	30.8
Fuel	a_g (s^{-1})/ T (K)			
M2				
Syn-5H ₂ 80N ₂	188±18/313	113±11/315	113±7/321	91±6/332
Syn-10H ₂ 80N ₂	438±25/314	383±11/323	288±6/315	224±5/327
Syn-1H ₂ 70N ₂	179±14/326	139±5/323	125±9/324	108±8/323
Syn-5H ₂ 70N ₂	495±25/328	439±9/320	301±6/321	270±5/331
Syn-10H ₂ 70N ₂	819±34/323	578±12/332	420±12/317	354±5/336
Syn-1H ₂ 60N ₂	395±10/321	312±4/327	269±5/324	262±7/333
Syn-1H ₂ 50N ₂	592±13/333	483±14/337	368±9/320	351±10/339
M1				
Syn-5H ₂ 80N ₂	255±13/421	216±7/404	168±2/423	141±8/396
Syn-10H ₂ 80N ₂	644±16/413	509±16/399	375±4/424	-/-
Syn-1H ₂ 70N ₂	304±9/467	270±7/469	251±5/484	175±3/454
Syn-5H ₂ 70N ₂	666±6/451	588±3/471	421±8/481	-/-

Table A.6: Global extinction strain (a_g) and burner temperature (T) data for Syn-H₂CO₂-air combinations

D (mm)	10.6	15.6	22.8	30.8
Fuel	a_g (s^{-1})/ T (K)			
M2				
Syn-5H ₂ 70CO ₂	275±13/314	196±10/311	173±8/309	163±5/315
Syn-10H ₂ 70CO ₂	549±28/316	368±8/312	266±16/311	263±9/313
Syn-1H ₂ 60CO ₂	207±13/319	172±10/312	145±11/310	126±9/314
Syn-5H ₂ 60CO ₂	520±12/323	394±10/326	286±15/311	280±4/316
Syn-1H ₂ 50CO ₂	392±25/324	341±9/315	295±7/311	261±9/313

Table A.7: Global extinction strain (a_g) and burner temperature (T) data for Syn1-N₂-air and Syn2-N₂-air combinations

D (mm)	10.6	15.6	22.8	30.8
Fuel	a_g (s^{-1})/ T (K)			
M2				
Syn1-65N ₂	604±24/318	434±4/313	295±9/313	280±3/309
Syn1-55N ₂	-/-	654±10/327	-/-	-/-
Syn2-70N ₂	629±21/313	447±8/312	301±5/312	276±5/308
Syn2-60N ₂	-/-	660±9/332	-/-	-/-

Table A.8: Global extinction strain (a_g) data for CH₄-air combination at three different distances

D (mm)	10.6	15.6	22.8	30.8
Distance (L)	a_g (s^{-1})			
M2				
6 cm	761±11	607±4	457±9	386±10
10 cm	765±2	610±2	469±4	384±4
12 cm	761±17	614±9	467±10	382±7

Table A.9: Global extinction strain (a_g) data for CH₄-air combination for wall effects

D (mm)	10.6	15.6	22.8	30.8
	a_g (s^{-1})			
M2				
with side wall	761±17	614±9	467±10	382±7
without side wall	768±11	620±7	478±14	387±3

Table A.10: Effect of insulation on global extinction strain (a_g) data for Syn-10H₂80N₂-air combination

D (mm)	10.6	15.6	22.8	30.8
	a_g (s^{-1})/ T (K)			
M2				
without insulation	438±25/317	383±11/323	288±6/315	224±5/327
with insulation	474±31/313	399±10/323	308±6/313	247±8/318

Table A.11: Effect of fuel flow rate on global extinction strain (a_g) data for Syn-5H₂80N₂-air combination using $D = 22.8$ mm

fuel flow	6 Lpm	8 Lpm	10 Lpm	12 Lpm	15 Lpm
Fuel	a_g (s^{-1})/ T (K)				
M2					
Syn-5H ₂ 80N ₂	74±4/312	91±4/315	96±2/318	114±8/321	116±6/318